

The ARTI Framework: Cosmic Rays Atmospheric Background Simulations

Christian Sarmiento-Cano¹, Mauricio Suárez-Durán², Rolando Calderón-Ardila¹, Adriana Vásquez-Ramírez³, Andrei Jaimes-Motta³, Luis A. Núñez³, Sergio Dasso^{4,5}, Iván Sidelnik⁶, Hernán Asorey^{a,1,7}, for the LAGO Collaboration⁸

¹Instituto de Tecnologías en Detección y Astropartículas (CNEA, CONICET, UNSAM), Centro Atómico Constituyentes, Buenos Aires, Argentina

²Université Libre de Bruxelles (ULB), Brussels, Belgium

³Escuela de Física, Universidad Industrial de Santander, Bucaramanga, Colombia

⁴Departamento de Ciencias de la Atmósfera y los Océanos, Facultad de Ciencias Exactas y Naturales, Grupo LAMP, Universidad de Buenos Aires, Buenos Aires, Argentina

⁵Instituto de Astronomía y Física del Espacio, Universidad de Buenos Aires (CONICET), Buenos Aires, Argentina

⁶Departamento de Física de Neutrones, Centro Atómico Bariloche, (CNEA, CONICET), Bariloche, Argentina

⁷Departamento de Física Médica, Centro Atómico Bariloche, (CNEA, CONICET), Bariloche, Argentina

⁸The LAGO Collaboration, see the complete list of authors and institutions at <http://lagoproject.net/collab.html>

Received: date / Accepted: date

Abstract ARTI is a complete framework intended to simulate the expected signals produced by the interaction of the secondary particles inside any Water Cherenkov Detector, WCD. ARTI comprises a simulation sequence by integrating three different simulation tools: a) magnetocosmics, to account for the geomagnetic field effects on the primary flux; b) CORSIKA, to simulate the atmospheric showers originated on the complete flux of cosmic rays in the energy range of interest and, thus, to estimate the expected flux of secondary particle at the site; and c) Geant4, for simulating the WCD detectors response to this secondary flux. In this work, we show the usage of the ARTI framework by calculating the expected flux of signals at eight sites from the Latin American Giant Observatory, LAGO. This covers a wide range of altitudes and geomagnetic rigidity cut-offs. This shows it is possible to estimate the secondary particle flux originated by cosmic rays at any location in the world. This flux could be used either to be injected into WCDs, to estimate the footprint generated by Gamma-Ray Burst events, or over a geological structure in muography applications.

Keywords Cosmic rays flux · Space weather · Muography

1 Introduction

The detection of secondary particles at ground level originated from the interaction of primary cosmic rays in the atmosphere, is one of the most commonly used techniques in astroparticle physics to obtain the observable related to the underlying physical processes. This technique can be used to study transient events such as gamma-ray bursts [1], Forbush decreases [2] and other applications such as muography [3,4]. Detailed knowledge of how the secondaries are produced in the atmosphere and how they reach a geographical position is needed to accomplish this main research goals. In this paper, we study the response of Water Cherenkov Detectors (WCD) to secondary particles in very different sites in Latin America, as shown in figure 1. Currently, several computational tools, such as Magnetocosmics (MAGCOS) [8] enables the computation of charged particles trajectories by using advanced and detailed geomagnetic field models. Furthermore, CORSIKA [6] or FLUKA [7], allow the estimation of the nominal flux of those particles arriving at ground level. This simulation tool is based on Monte Carlo methods and in our implementation we take into account the complete measured spectra of Galactic Cosmic Rays (GCR). To evaluate the response of the whole system, a reliable simulation of the detector response to this background radiation is needed. This requires the use of very powerful computational tools such as Geant4 [9].

^ae-mail: hernan.asorey@iteda.cnea.gov.ar

The integration of these computational tools allows the design of new observatories for GCR as well as to develop physical models to understand how the observed time variability on the time evolution of the measured signals might be correlated with perturbations on the nominal GCR flux, such as, e.g., the prompt detection of the high energy component of gamma-ray bursts or space weather and space climate related activity. For this reason, detecting cosmic radiation and using it to study astroparticles and geophysical phenomena are one of the main goals of the Latin American Giant Observatory (LAGO) [10].

To appraise the expected performance of different detectors and sites, we have developed ARTI¹, a full computational framework to estimate the signals expected at any site in any atmospheric and geomagnetic conditions and for any detector geometry and configuration. This toolkit is the final result of the developments we started at LAGO to assess the effect of the evolving geomagnetic field conditions in the propagation of low energy GCR [17], that now includes also the local atmospheric status using the Global Data Assimilation System (GDAS) model [18] and the detector response using Geant4.

The outline of this document is as follows: in section 2 we introduce the method implemented for estimate the nominal background radiation at the detector level. Then, in section 3, we explain the methodology used to implement the correction by the geomagnetic field condition, at eight representative locations of the LAGO sites [12,20]. The expected signals from a unique standard WCD, were modeled using Geant4 to allow a direct comparison among different sites using the same WCD geometry. The resulting calculations are presented for each of these eight sites in Section 4. Finally, in Section 5, final remarks and future perspectives of this work are discussed.

2 Cosmic background radiation at ground level

The flux of secondary particles at ground level was obtained for each LAGO site following the method detailed described in [17]. In this method, the GCR flux (Φ) is calculated as an isotropic flux at the top of the Earth's atmosphere, at an altitude of 112 km a.s.l. [19], where Φ is defined as

$$\Phi(E_p, Z, A, \Omega) \simeq j_0(Z, A) \left(\frac{E_p}{E_0} \right)^{\alpha(E_p, Z, A)}, \quad (1)$$

and E_p is the energy of the particle, $\alpha(E_p, Z, A)$ is considered constant, i.e. $\alpha \equiv \alpha(Z, A)$, in the energy range

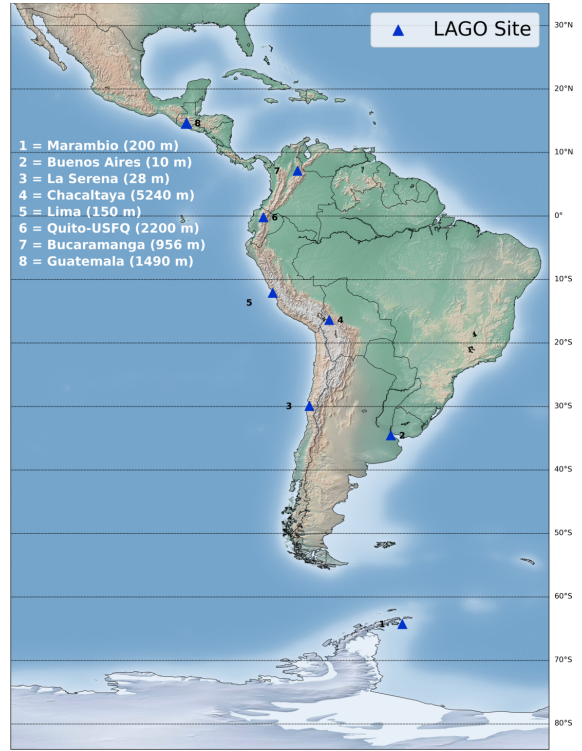


Fig. 1 Geographical distribution and altitudes of the Latin American Giant Observatory water Cherenkov detectors: the ones in operation are represented with blue triangles, orange squares are those in deployment and the planned sites are indicated in red circles. In this work we studied eight representative locations referenced by latitude and altitude as follows (Latitude, Altitude): Buenos Aires, Argentina (-34.54° , 10 m a.s.l.); Lima, Perú (-12.1° , 150 m a.s.l.); Ciudad de Guatemala, Guatemala (14.63° , 1490 m a.s.l.); Bucaramanga, Colombia (7.14° , 956 m a.s.l.); Quito, Ecuador (-0.2° , 2800 m a.s.l.); Chacaltaya, Bolivia (-16.35° , 5240 m a.s.l.); La Serena, Chile (-29.90° , 28 m a.s.l.), and the Argentinian antarctic Base Marambio, at the Antarctica Peninsula, where one LAGO detector has been working since the beginning of 2019 (-64.24° , 200 m a.s.l.).

of interest for this work, from a few GeV to 10^6 GeV, and $E_0 = 10^3$ GeV. For each kind of GCR considered, $\alpha(Z, A)$, is individualized by its mass number (A) and atomic number (Z) and $j_0(Z, A)$ is the normalization parameter.

To improve the global computational efficiency, the first stage of ARTI uses CORSIKA [6] to calculate the expected flux of secondary particles produced by the interaction of each GCR with the atmosphere [6] at the detector level for each LAGO site. In this case, we uses CORSIKA v7.6500 compiled with the following options: QGSJET-II-04 [22]; GHEISHA-2002; EGS4; curved and external atmosphere and volumetric detector. The IGRF-12 model [23] is used to provide the local geomagnetic field values, B_x and B_z , required by COR-

SIKA to take into account the geomagnetic effects on the particle propagation in the atmosphere.

To calculate the expected number of primaries to be simulated, we integrate Φ for each type of primary from proton to iron (i.e., $1 \leq Z \leq 26$) in time (typically from one hour to one day of flux), area (typically 1 m^2), solid angle (typically $0 \leq \theta \leq \pi/2$ and $0 \leq \phi \leq 2\pi$ where θ and ϕ are the zenithal and azimuthal angles respectively), and energy (typically from the minimum value of the local rigidity cut-off times Z up to 1 PeV , see the next section). It is important to notice that the integrated flux is simulated following the corresponding distribution for each type of particle [12, 14, 17].

During the simulation, each secondary particle is tracked down to the lowest energy threshold that CORSIKA allows depending on the type of the secondary. Currently, these threshold are $E_s \geq 5 \text{ MeV}$ for μ^\pm s and hadrons (excluding π^0 s); and $E_s \geq 5 \text{ keV}$ for e^\pm s, π^0 s and γ s, where E_s is the energy of secondary particle. Since the atmospheric profile is a key factor for the production of secondary particles, and a parameter for CORSIKA, we have to set atmospheric external profile models [24] according to the geographical position of the LAGO sites: a tropical profile for Bucaramanga (BGA, Colombia), Ciudad de Guatemala (GUA, Guatemala) and Quito (UIO, Ecuador), a subtropical profile [18] for Buenos Aires (EZE, Argentina), Lima (LIM, Perú), La Serena (LSC, Chile) and Chacaltaya (CHA, Bolivia), and the antarctic profile for the Marambio Base (SAWB, Antarctica) [20, 25]. In our implementation, these profiles can be updated by using the GDAS system to use the local atmospheric conditions [18].

All the primary simulation parameters, including the integration time and area, the energy ranges, the solid angle, the site altitude and geomagnetic coordinates, and several others parameters can be independently set by the user in ARTI. With all this information ARTI creates several CORSIKA data files² and different scripts to run the corresponding simulations. Currently ARTI supports different types of clusters architectures, and even it runs on distributed computational solutions such as those based on GRID or CLOUD based implementations[44].

In this work, the secondary flux of particles at ground, Ξ , has been calculated for each of the eight LAGO sites mentioned earlier. In figure 2, we show the results obtained for the expected secondary spectra at four representative sites: CHA (5240 m a.s.l.), LSC (28 m a.s.l.), LIM (150 m a.s.l.) and SAWB (200 m a.s.l.). As expected, there are fewer particles at low altitude due

to atmospheric absorption. Namely, the flux at CHA is larger than the one at LSC for each type of secondary.

3 Geomagnetic field corrections

Low energy GCRs ($E_p < 100 \text{ GeV}$) trajectories are deflected by the Earth magnetic field (GF). The deflection is parametrized by the magnetic rigidity term (R_m) [26, 27, 28]. For instance, transient solar phenomena, such as Forbush decrease (FD) events are decreases of CRs fluxes originated in interplanetary structures near Earth. During these events, the geomagnetic field can be also perturbed due to its interaction with the magnetized solar wind plasma, and consequently change the geomagnetic shielding on energetic particles, and modifies its trajectory. Thus, it can change in the cosmic background radiation at ground level [29, 2, 30]. Several FD events have been registered by different observatories using WCDs [31, 30, 32, 10, 33, 14]. In this sense, the LAGO Collaboration have developed the LAGO Space Weather (LAGO-SW) program [10, 14], to study the variations in the flux of secondary particles at ground level and their relation to the heliospheric modulation of GCRs [17]. The GF effect on the flux Ξ has been included in this work for each of the eight selected LAGO sites, following the LAGO-SW methods, i.e., by filtering at this second stage of the ARTI framework the secondaries produced by those GCRs that can not reach the respective location as a function of its rigidity. These methods allow us to determine the expected background flux baseline and to evaluate the impact of the changing geomagnetic conditions during, for example, a geomagnetic storm [17].

It is important to remark that this method uses the local magnetic rigidity cut-off (R_c) defined as,

$$R_c = R_c(\text{Lat}, \text{Lon}, \text{Alt}, t, \theta, \phi, P(R_m((\theta), t))), \quad (2)$$

as a function of the geographical latitude (Lat), longitude (Lon), altitude above sea level (Alt), and primary arrival direction (θ, ϕ), time t , including a cumulative probability distribution function for the penumbra region, ($P(R_m((\theta), t))$), as explained in [17].

The results for the estimated flux of cosmic background radiation at ground level, including the GF correction, for the eight LAGO sites are presented in Table 1. Here, it can be seen how the altitude of the site is the predominant variable over the total flux of secondary particles (Ξ). This effect can be also seen in Figure 3, which shows the two effects: atmospheric and geomagnetic shielding (i.e., altitude and latitude dependence) at some representatives sites. As an example of this, it can be seen that the total flux at Chacaltaya

²A specially formatted ASCII file containing all the parameters needed to run the corresponding CORSIKA simulation.

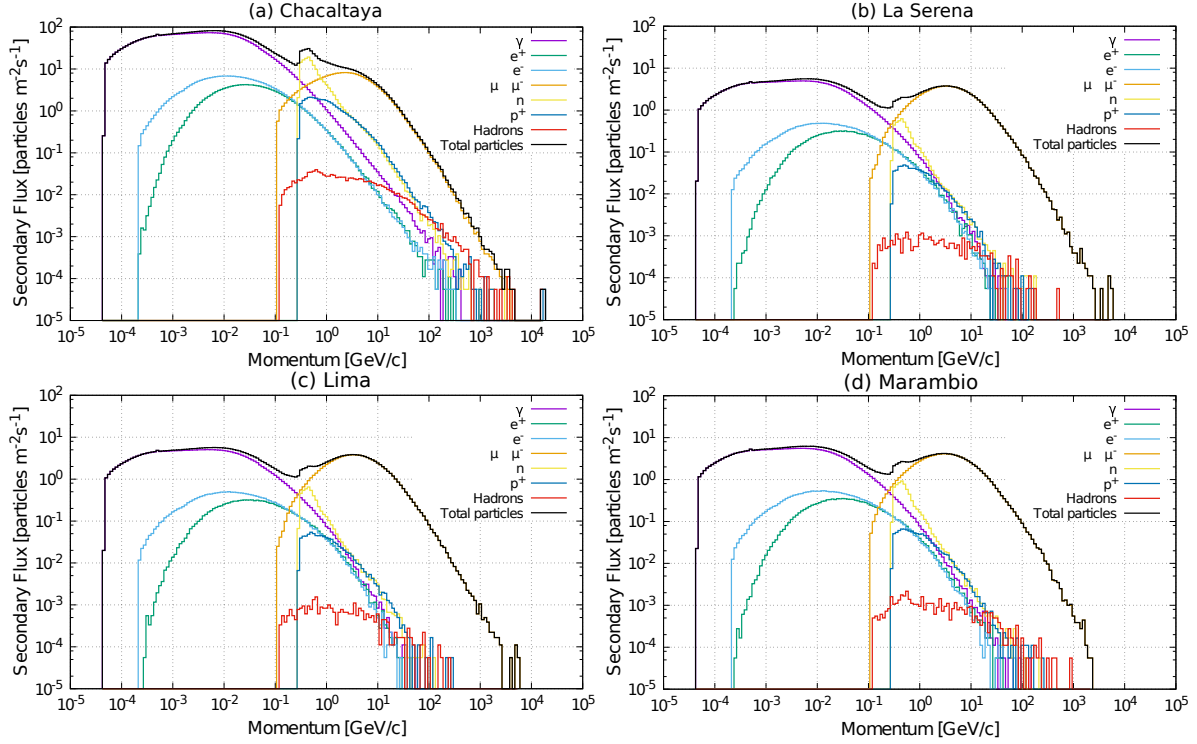


Fig. 2 The spectrum of the secondary particles at four LAGO sites: (a) Chacaltaya (CHA), Bolivia (5240 m a.s.l.); (b) La Serena (LSC), Chile (28 m a.s.l.); (c) Lima (LIM), Perú (150 m a.s.l.) and (d) Marambio Base (SAWB), Antarctica (200 m a.s.l.). The comparison of these four plots put in evidence a difference of one order of magnitude (at $\sim 10^{-2}$ GeV/c) in the total of secondaries (black line). At $\sim 3.5 \times 10^{-1}$ GeV/c between Chacaltaya y La Serena, the neutron component (yellow line at 0.5 GeV) for Chacaltaya dominates over the μ^\pm component (orange line), while for the La Serena estimation is the opposite. Since the LAGO detectors calibrations are based on the muons, it is important to note that the prediction for the muon component is larger than for the e^\pm (green and blue lines) ones at La Serena; meanwhile, at Chacaltaya, e^\pm dominates with respect to μ^\pm due to atmospheric development of the cascades.

(5240 m a.s.l.) is almost 10 times greater when we compare it to Bucaramanga (956 m a.s.l.). By the other hand, as expected due to that the geomagnetic effect filters only the low energy primary particles, the dependence of the total secondary particle flux with the geographical latitude is in general less abrupt, but still important. However, the geomagnetic effect on the flux of secondary neutrons is dramatic, as can be seen in the right panel of Figure 3. This Figure shows a comparison of the flux of electromagnetic particles (γ, e^\pm), muons (μ^\pm) and neutrons (n), at four sites with similar altitude but very different geomagnetic rigidities: Marambio (SAWB, 200 m a.s.l., 2 GV/c), Buenos Aires (EZE, 10 m a.s.l., 8 GV/c), La Serena (LSC, 28 m a.s.l., 9 GV/c), and Lima (LIM, 150 m a.s.l., 12 GV/c). This considerable latitudinal dependence of the flux of secondary neutrons, combined with the capacity of WCDs to indirectly observe neutrons [38], has as a major impact for space weather studies and it strongly supports the installation of WCD at sites with very low rigidity cut-off, such as those that LAGO deployed at the Antarctic continent. Further investigations of the un-

derlying mechanisms are underway within our Collaboration and will be published in a separate work.

4 Water Cherenkov detector simulation

The third stage of ARTI is the LAGO-GD package, a complete and detailed simulation of the typical LAGO water Cherenkov detector based on Geant4 [9]. This framework allows us to obtain a precise and detailed simulation of the interaction between the particle flux at the detector level obtained in the previous stage. The LAGO WCDs are typically cylindrical containers with approximately $1m^3$ to $4m^3$ of pure water, with an inner coating made of Tyvek®, a water tight and UV light reflective and diffusive material [34, 35]. Usually, a single 8" or 9" photomultiplier tube (PMT) is at the center of the top of the cylinder pointing downwards and in close contact with the water surface [36, 10, 11]. Data acquisition and detector slow control is carried out by means of an own designed electronics [37].

LAGO-GD starts with the estimated flux Ξ , and places all the particles on a circular area A , just above

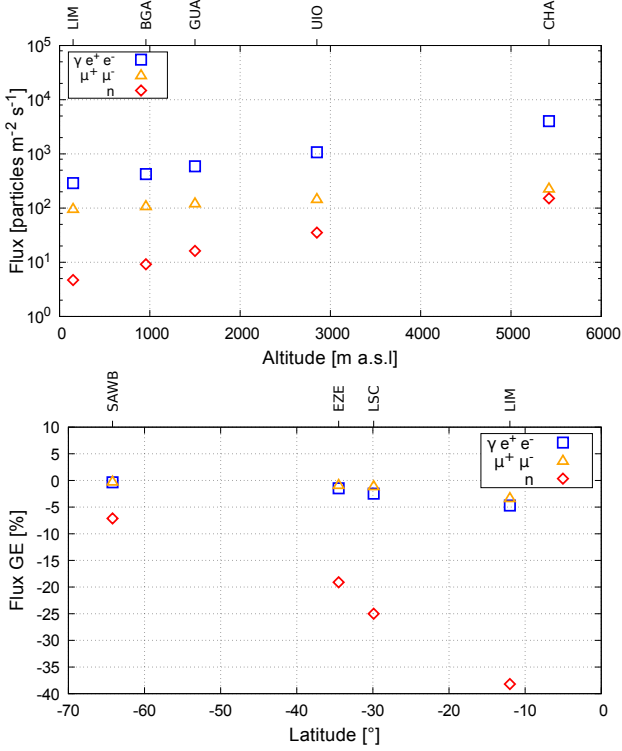


Fig. 3 The flux (Ξ) of cosmic background radiation at ground as a function of the altitude at five LAGO sites with very different altitude but similar geomagnetic rigidities is shown in the left panel for different components of the cascades: the electromagnetic component in blue squares (γ , e^- , e^+), the muonic component in yellow triangles (μ^- , μ^+) and neutrons as part of the hadronic component are shown in red diamonds (n). The altitude effect on the flux is clearly visible. Instead, in the right panel, the same flux is shown as a function of the geomagnetic rigidity for four LAGO sites with similar altitudes but very different values of the rigidity cut-offs. While the effect on the total flux is not as big as the altitude effect, the impact of the latitude on the neutron flux is quite significant.

the WCD, during a time t . For any geometrical configuration for the detector, a model of the container internally coated by a Tyvek-like surface and filled with pure water is built. The passage of ultra-relativistic charged particles through the detector produce photons through the well known Cherenkov effect. One of the main advantages of large volume detectors such as the WCDs is based on their capabilities to detect neutral components of the extensive air showers that reach the ground, such as photons or neutrons. Secondary photons are detected by pair creation, photoelectric effect and, mainly, the Compton effect in the large water volume, which in turn produces relativistic electrons capable of produce Cherenkov light. While neutrons are indirectly detected by photons produced after a thermalized neutron is captured in the water volume [38].

Table 1 Flux of cosmic background radiation at ground level estimated at eight LAGO sites: Chacaltaya, Bolivia (CHA); Quito, Ecuador (UIO); Ciudad de Guatemala (GUA); Bucaramanga, Colombia (BGA); Marambio Base, Antarctica (SAWB); Lima, Perú (LIM); La Serena, Chile (LSC) and Buenos Aires, Argentina (EZE). The total flux for all secondaries (Ξ^{All}) is presented along with the relative geomagnetic effect over the total flux (noted as GE^i [%]), estimated as the percent difference with respect to the flux Ξ without considering the GF effect.

LAGO site	Alt [m a.s.l.]	R_C GV/c	Ξ^{All} [$\text{m}^{-2} \text{s}^{-1}$]	GE^{All} [%]
CHA	5240	11.6	4450	-17.7
UIO	2800	12.2	1260	-11.6
GUA	1490	9.1	730	-4.2
BGA	956	11.6	540	-5.9
SAWB	200	2.2	430	-0.4
LIM	150	12.0	390	-4.8
LSC	28	9.3	380	-2.6
EZE	10	8.2	390	-1.5

All those Cherenkov photons propagate inside the detector and can be absorbed in the water volume or in the internal coating, or eventually, reach the sensitive surface of the PMT. At the center of the cylinder and almost fully immersed in the water surface, the PMT is modelled just as a semi-ellipsoid sensitive surface. The PMT response is simulated by a simple Metropolis-Hastings algorithm and using the reported quantum efficiency dependence on the photon wavelength provided by the PMT manufacturer, typically below 25-30%. If the photon is converted, the resulting photo-electron number, pe , and the corresponding impinging time are registered as a pulse with an acquisition system.

As mentioned above, in this work we simulate the same standard LAGO WCD for all the studied sites to allow a direct comparison of the effect of the altitude and geomagnetic field effects. This detector is composed by a plastic water commercial container of 2.1 m diameter and 0.90 m height, filled with 3.12 m³ of pure water and internally fully coated with a single Dupont® Tyvek® layer. For the PMT, a Hamamatsu R5912 [39] was used with and corresponding ellipsoid geometry semi-axis ($a_x = 101$ mm; $Rb_y = 101$ mm, $c_z = 65$ mm).

Once the geometry of the detector is fixed, in order to convert the number of pe to the corresponding physical units of deposited energy E_d within the detector, we use the same calibration procedure that is commonly used for WCD [12, 40, 41]. According to this method, the main property of the measured signal by the detector is the charge associated with the pulse produced by a central and vertical muon going

through the detector. This is the so called VEM, for Vertical Equivalent Muon. In the left panel of the Figure 4 a sketch of the simulated detector with a vertical muon moving downwards through the water volume is shown. Since in this energy range secondary muons present a nearly constant energy loss of $2 \text{ MeV cm}^2 \text{ g}^{-1}$, i.e., 2 MeV cm^{-1} in water, it is quite simple to establish the single-photo-electron to deposited energy equivalence: a signal of 1 VEM correspond to a deposited energy of $E_d^{\text{VEM}} = 2 \times h \text{ MeV}$, where h is the detector water volume height measured in cm. In general, the VEM value is obtained from the histogram of the total charge deposited in the PMT after some geometrical corrections [40].

Geometry and detector response to the different components of the extensive air shower produce a characteristic peak both in the simulated and in the measured charge histograms that corresponds to the signals associated to muons, and in particular, the value of the VEM is easily identifiable as a characteristic hump in the histogram [40, 42]. This same schema was implemented in the LAGO-GD code. First, the number of pe produced by a single VEM was calculated. The expected distribution of pes obtained for 10^5 vertical muons of $E = 3 \text{ GeV}$ impinging at the center of the detector is shown in figure 4. In this case, the peak of the distribution is fitted to obtain the most probable number of pe for a single VEM, obtaining our main calibration parameter: $1 \text{ VEM} \simeq 100 pe \simeq 180 \text{ MeV}$, as $h = 90 \text{ cm}$ in our simulated WCD. Once the calibration equivalence is obtained, the response of the detector to the different components of the secondary particles flux Ξ is calculated and the corresponding total signal histograms (charge histograms) are built. The resulting histograms for the LAGO sites of Chacaltaya (Bolivia, 5240 m a.s.l.), La Serena (Chile, 28 m a.s.l.), Lima (Perú, 150 m a.s.l.) and Marambio (Antarctica, 200 m a.s.l.) are shown in the Figure 5. The histogram is composed by the individual contribution of all the particles detected by the WCD presented in the shower. The calorimetric-like behaviour [43] of the WCD is visible in the low energy sector of the histograms ($E_d \leq 150 \text{ MeV}$), where the main contributions come from electromagnetic particles (γ and e^\pm) in the cascade. Muons at the VEM energy scale ($150 \text{ MeV} \leq E_d \leq 300 \text{ MeV}$) or greater ($E_d \geq 300 \text{ MeV}$) are dominated by single muons and multiple simultaneous particles respectively. The low energy loss for muons when compared to their total energy explains this behavior, as the vast majority of muons posses enough energy to full traverse the detector and beyond. So, for muons, signals are not calorimetric, i.e., the total signal is not proportional to the muon total energy, as it is for electrons, but depends

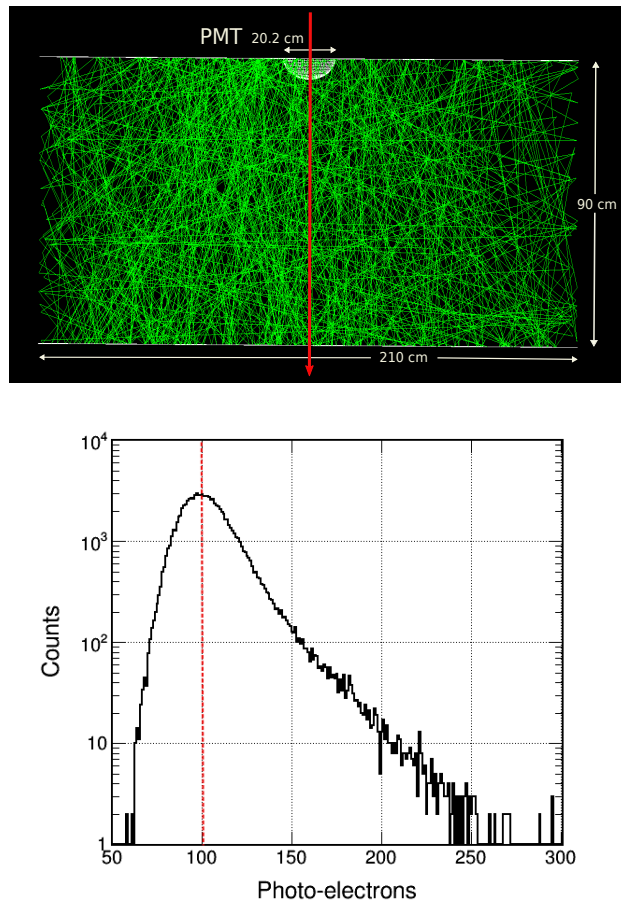


Fig. 4 Left: A vertical and central muon of 3 GeV (red arrow) goes through the detector producing thousands of Cherenkov photons (green lines) that are propagated in the water volume and diffusively reflected in the Tyvek® coating. After some time, these photons can be absorbed or finally reach the PMT, producing a certain number of photoelectrons (pe). Right: The distribution of the number of pe obtained for 10^5 central and vertical muons of 3 GeV obtained with the LAGO-GD simulation. The peak of the expected number of photoelectrons, 100 pe , represents the main unit of calibration for this particular simulated detector geometry and it is proportional to the VEM deposited signal. In this case, $1 \text{ VEM} \simeq 100 pe \simeq 180 \text{ MeV}$ of deposited energy.

only on the muon trajectory and the total length traveled inside the water volume. In Table 2, the rate of particles detected (Ξ^D) and its contribution to the total deposited energy are shown.

To analyze the direct impact of the altitude on the expected signals and the histogram shape on real data from very different detectors at different sites is a complicated problem, and powerful data analysis techniques including machine learning approaches are being carried out within our collaboration to asses this task. Also, these results are useful for such analysis, as the development of the extensive air showers have different

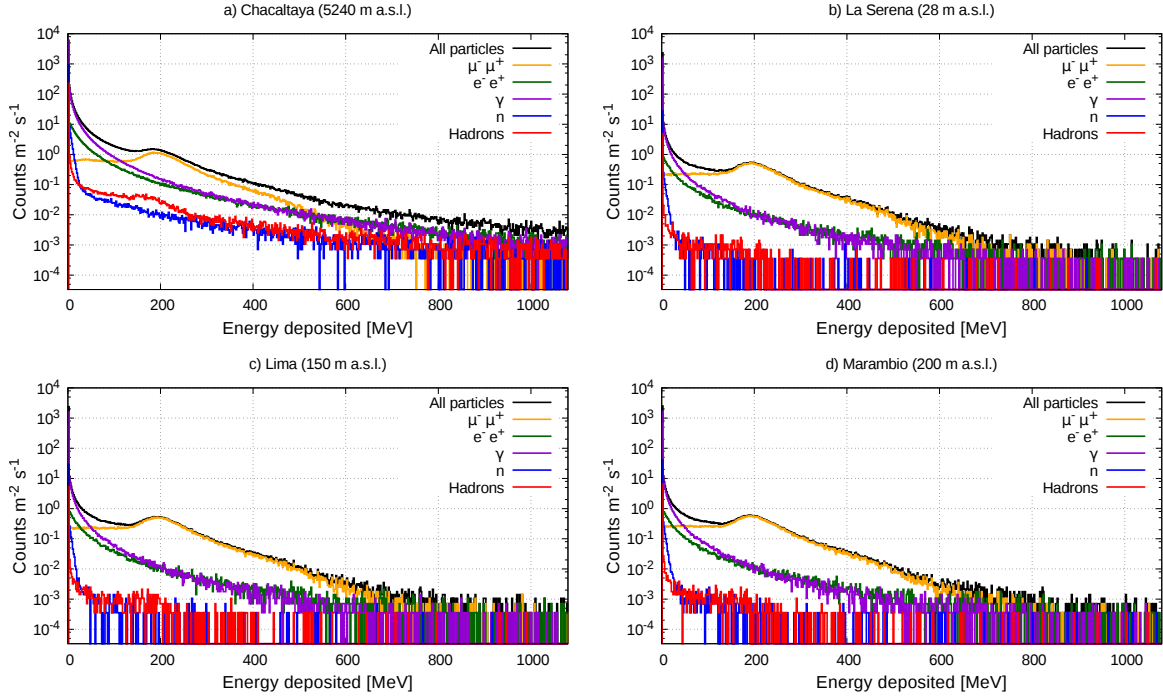


Fig. 5 Charge histograms of the total signal (black line) and single component contributions (color lines) are shown for four LAGO sites: Chacaltaya (a), La Serena (b), Lima (c) and Marambio (d). The histograms have been normalized to areas of 1 m^2 and exposure time of 1 second.

Table 2 Expected rate background radiation, Ξ^D , that can be detected in a single WCD like the one described in this work at eight LAGO sites (see the table 1 for the characteristic of each location). The deposited energy for the different components of the extensive air showers is also shown: electromagnetic component E_d^{EM} , muon component E_d^μ , neutrons E_d^n , and the total deposited energy E_d^{All} . Please note that for the hadronic component we only show the neutron contribution. The remaining hadronic contribution can be obtained by subtraction.

LAGO Site	$\Xi^D [\text{m}^{-2} \text{s}^{-1}]$	$E^{\text{EM}} [\text{GeV}]$	$E^\mu [\text{GeV}]$	$E^n \times 10^{-1} [\text{GeV}]$	$E^{\text{All}} [\text{GeV}]$
CHA	1800	1.49	0.22	0.49	1.77
UIO	520	0.40	0.14	0.11	0.55
GUA	310	0.22	0.11	0.05	0.34
BGA	230	0.16	0.10	0.03	0.26
LSC	170	0.11	0.09	0.01	0.20
LIM	170	0.11	0.09	0.02	0.20
EZE	170	0.11	0.09	0.01	0.20
SAWB	180	0.11	0.10	0.02	0.21

maximum for each component, and so, the component-to-muon ratio of the deposited energy within the detector can be used to study the detector performance at different altitudes. As an example, in Figure 6 it is possible to see these relative ratios for the number of photons, electrons, neutrons and other hadrons respect to number of muons, as a function of the site altitude. As expected, as we approach sea level the muon impact becomes higher, while very high altitude sites such

as Chacaltaya are better to detect the electromagnetic branch initiated in the cascades.

5 Conclusions

In this work, the ARTI framework capabilities are presented using eight different LAGO sites as practical example. LAGO is a very large baseline array of water Cherenkov detectors, that spans from the high altitude

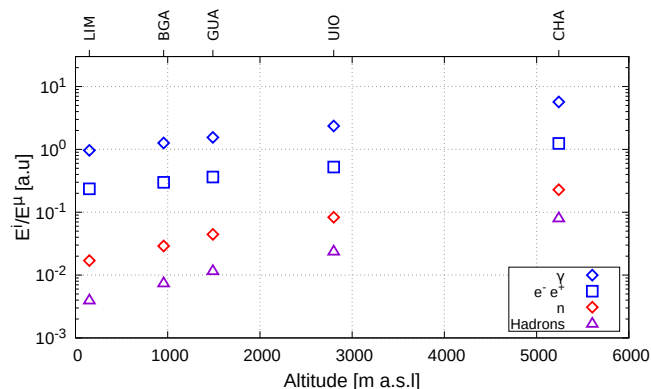


Fig. 6 The component-to-muon ratio, i.e., the ratio between the deposited energy within the detector volume by a particular shower component (photons, blue diamonds; electrons, blue squares; neutrons, red diamonds; and hadrons, violet triangles) divided by the energy deposited by muons, is shown for five LAGO sites with similar geomagnetic rigidity but increasing altitude: Lima (LIM), Bucaramanga (BGA), Guatemala city (GUA), Quito (QUI) and Chacaltaya (CHA). The observed trend for this ratio reflects the expected evolution of the cascades with altitude as the impact of the atmospheric absorption is much lower for muons than for other showers components. It is clear that high altitude sites are optimal for the study of photon initiated showers, such as those produced by GRBs.

mountains of the Andes Range at the south of Mexico to the frozen plateaus of Antarctic Peninsula. By design, the detection network was deployed at similar geographic longitudes, but very different latitudes (and so, different values of the geomagnetic rigidity cutoffs) and altitudes (and so, different atmospheric depths). Space weather and climate, high energy component of gamma-ray bursts and detailed analysis of the background radiation at surface level are some of the scientific objectives of this collaborative detection network. Moreover, the usage of water Cherenkov detectors assure the sensitivity to the main components of extensive air showers, improving the analysis of the transient impacts at different values of deposited energy.

To characterize this detection network, we developed, tested and verified ARTI, a very detailed simulation package, and some of its capabilities and results were described here. As an example, the altitude and geomagnetic rigidity cutoff effects were evaluated by comparing the expected flux of signals at eight different LAGO sites, with altitudes ranging from sea level up to more than five thousands meters above sea level, and for very low geomagnetic rigidities for sites near the Antarctic oval to very high rigidities for sites near the geomagnetic equator.

By using the ARTI simulation framework, it is possible to obtain the detailed flux of the expected background radiation, the detector signals or the radiation

doses above and at ground level, in any place in the World and under time-evolving atmospheric and geomagnetic conditions. ARTI gives the possibility of calculate a more detailed and statistically significant secondary particles spectra at ground at different energies, that can be used not only for the characterization of new astroparticle detection sites, including the particle detector, but also for the design of, e.g., better shielding for sensitive electronics, such as avionics or high performance computing facilities, and for conducting feasibility studies at underground laboratories or muography on large artificial structures such as hydroelectric or geological structures such as volcanoes.

6 Acknowledgment

The LAGO Collaboration is very grateful to all the participating institutions and to the Pierre Auger Collaboration for their continuous support. In addition, some results presented in this paper were carried out using the GridUIS-2 experimental test bed, being developed under the Universidad Industrial de Santander (SC3UIS) High Performance and Scientific Computing Center, development action with support from UIS Vicerrectoria de Investigación y Extension (VIE-UIS) and several UIS research groups as well as other funding bodies. Other calculations were performed at the simulation cluster of ITeDA. The authors are grateful to Adrian José Pablo Sedoski for his continuous technical support.

References

1. K. Hurley, B. Dingus, R. Mukherjee, P. Sreekumar, C. Kouveliotou, C. Meegan, G. J. Fishman, D. Band, L. Ford, D. Bertsch, et al, *Detection of a γ -ray burst of very long duration and very high energy*, Nature **372** (1994) 652-654
2. I. G. Usoskin, I. Braun, O. G. Gladysheva, J. R. Hörandel, T. Jämsén, G. A. Kovaltsov, S. A. Starodubtsev, *Forbush decreases of cosmic rays: Energy dependence of the recovery phase*, Journal of Geophysical Research: Space Physics **113** (2008)
3. K. Jourde, D. Gibert, J. Marteau, J. de Bremond d’Ars, S. Gardien, C. Girerd, J. Ianigro, *Monitoring temporal opacity fluctuations of large structures with muon radiography: a calibration experiment using a water tower*, Scientific Reports **6** (2016)
4. K. Morishima, M. Kuno, A. Nishio, N. Kitagawa, Y. Manabe, M. Moto, F. Takasaki, H. Fujii, K. Satoh, H. Kodama, et al, *Discovery of a big void in khufu pyramid by observation of cosmic-ray muons*, Nature **552** (2017) 386
5. A. Vázquez-Ramírez, M. Suárez-Durán, A. Jaimes-Motta, R. Calderón-Ardila, J. Peña-Rodríguez, J. Sánchez-Villafrades, J. Sanabria-Gómez, H. Asorey, L. Núñez,

- Simulated response of MuTe, a hybrid Muon Telescope*, Journal of Instrumentation **15** (08) (2020)
6. D. Heck, J. Knapp, J. N. Capdevielle, G. Schatz, T. Thouw, *CORSIKA: a Monte Carlo code to simulate extensive air showers*, FZKA-6019, www-ik.fzk.de/corsika (1998)
 7. A. Ferrari, P. Sala, A. Fasso, J. Ranft, U. Siegen et al, *Fluka: A multi-particle transport code*, Stanford Linear Accelerator Center (SLAC) (2005)
 8. L. Desorgher, *MAGNETOSCOSMICS, Geant4 application for simulating the propagation of cosmic rays through the Earth magnetosphere*, Technical report, Physikalisches Institut, University of Bern, Bern, Germany (2003)
 9. S. Agostinelli, J. Allison, K. Amako, J. Apostolakis, et al, *Geant4 - a simulation toolkit*, Nuclear Instruments and Methods in Physics Research Section A: Accelerators, Spectrometers, Detectors and Associated Equipment **506** (2003) 250–303
 10. H. Asorey and the LAGO Collaboration, *The LAGO Solar Project*, Proceedings of the 33th International Cosmic Ray Conference ICRC, Rio de Janeiro, Brasil (2013)
 11. I. Sidelnik and the LAGO Collaboration, *The sites of the Latin American Giant Observatory*, The 34th International Cosmic Ray Conference, volume PoS (ICRC2015) (2015) 665
 12. W. Alvarez, et al., *The Latin American Giant Observatory: Contributions to the 34th International Cosmic Ray Conference (ICRC 2015)*, arXiv:1605.02151 (2016)
 13. H. Asorey, S. Dasso, the LAGO Collaboration, *LAGO: the Latin American Giant Observatory*, The 34th International Cosmic Ray Conference, volume PoS (ICRC2015) (2015) 247
 14. H. Asorey, S. Dasso, L. A. Núñez, et al., for the LAGO Collaboration, *The LAGO space weather program: Directional geomagnetic effects, background fluence calculations and multi-spectral data analysis*, The 34th International Cosmic Ray Conference, volume PoS (ICRC2015) (2015) 142
 15. H. Asorey, P. Miranda, A. Núñez-Castiñeira, et al, for The LAGO Collaboration, *Analysis of background cosmic ray rate in the 2010-2012 period from the LAGO detectors at chacaltaya*, The 34th International Cosmic Ray Conference, volume PoS (ICRC2015) (2015) 414
 16. A. Vesga-Ramírez, D. Sierra-Porta, et al., *Muon Tomography sites for Colombian volcanoes*, arXiv:1705.09884 (2017)
 17. H. Asorey, L.A. Núñez, M. Suárez-Durán., *Preliminary results from the Latin American Giant Observatory space weather simulation chain*, Space Weather **16** (2018) 461–475
 18. J. Grisales-Casadiegos, C. Sarmiento-Cano and L. A. Núñez., *Impact of Global Data Assimilation System atmospheric models on astroparticle showers*, Canadian Journal of Physics (2021)
 19. M. Aguilar, J. Alcaraz, J. Allaby, et al., *Relative composition and energy spectra of light nuclei in cosmic rays: results from AMS-01*, The Astrophysical Journal **724** (2010) 329
 20. S. Dasso, A. Gulisano, J. Masías-Meza, H. Asorey, the LAGO Collaboration, *A project to install water-Cherenkov detectors in the antarctic peninsula as part of the LAGO detection network*, The 34th International Cosmic Ray Conference, volume PoS (ICRC2015) (2015) 105
 21. A. Letessier-Selvon, T. Stanev, *Ultrahigh energy cosmic rays*, Rev. Mod. Phys. **83** (2011) 907–942
 22. S. Ostapchenko, *Monte Carlo treatment of hadronic interactions in enhanced Pomeron scheme: QGSJET-II model*, Physical Review D **83** (2011) 014018
 23. E. Thébault, C. C. Finlay, C. D. Beggan, P. Alken, J. Aubert, O. Barrois, F. Bertrand, T. Bondar, A. Boness, L. Brocco, et al. *International geomagnetic reference field: the 12th generation*, Earth, Planets and Space **67** (2015) 79
 24. F. X. Kneizys, L. W. Abreu, G. P. Anderson, J. H. Chetwynd, et al. *The MODTRAN 2/3 report and LOW-TRAN 7 model*, Technical Report, 1996
 25. J.J. Masías-Meza and S. Dasso, *Geomagnetic effects on cosmic ray propagation under different conditions for Buenos Aires and Marambio, Argentina.*, SunGe **9** (2014) 41–47
 26. D. Smart, M. Shea, *Fifty years of progress in geomagnetic cutoff rigidity determinations*, Advances in Space Research **44** (2009) 1107–1123
 27. R. Modzelewska, M. Alania, *The 27-day cosmic ray intensity variations during solar minimum 23/24*, Solar Physics **286** (2013) 593–607
 28. J.J. Masías-Meza, S. Dasso, P. Démoulin, L. Rodríguez, M. Janvier, *Superposed epoch study of icme substructures near earth and their effects on galactic cosmic rays*, Astronomy & Astrophysics **592** (2016) A118
 29. H. Cane, *Coronal Mass Ejections and Forbush Decreases*, Space Science Reviews **93** (2000) 55–77
 30. H. Asorey for the Pierre Auger Collaboration, *Measurement of Low Energy Cosmic Radiation with the Water Cherenkov Detector Array of the Pierre Auger Observatory*, Proceedings of the 33th ICRC, Beijing, China, (2011) 41–44
 31. I. Angelov, E. Malamova, J. Stamenov, *The forbush decrease after the GLE on 13 december 2006 detected by the muon telescope at BEO-moussala*, Advances in Space Research **43** (2009) 504–508
 32. S. Dasso, H. Asorey, Pierre Auger Collaboration, *The scaler mode in the pierre auger observatory to study heliospheric modulation of cosmic rays*, Advances in Space Research **49** (2012) 1563–1569
 33. M. Mostafá, for the HAWC Collaboration, *The high-altitude water cherenkov observatory*, Brazilian Journal of Physics **44** (2014) 571–580
 34. A. Filevich, P. Bauleo, H. Bianchi, J. Martino, G. Torlasco, *Spectral-directional reflectivity of tyvek immersed in water*, Nuclear Instruments and Methods in Physics Research Section A: Accelerators, Spectrometers, Detectors and Associated Equipment **423** (1999) 108–118
 35. R. Calderón, H. Asorey, L.A. Núñez, The LAGO Collaboration, *Geant4 based simulation of the Water Cherenkov Detectors of the LAGO Project*, Nuclear and Particle Physics Proceedings **267** (2015) 424–426
 36. D. Allard, I. Allekotte, C. Alvarez, et al., *Use of water-Cherenkov detectors to detect gamma-ray bursts at the large aperture GRB observatory (LAGO)*, Nuclear Instruments and Methods in Physics Research Section A: Accelerators, Spectrometers, Detectors and Associated Equipment **595** (2008) 70–72
 37. M. Sofo-Haro, L. H. Arnaldi, W. Alvarez, et al., *The data acquisition system of the Latin American Giant Observatory (LAGO)*, Nuclear Instruments and Methods in Physics Research Section A: Accelerators, Spectrometers, Detectors and Associated Equipment **820** (2016) 34–39
 38. I. Sidelnik, H. Asorey, N. Guarín, M. Suárez-Durán, et al, *Enhancing neutron detection capabilities of a water Cherenkov detector*, NIM A **955** (2020) 163172

- 39. W. Wang, S. Qian, J. Xia, Z. Ning, Y. Cheng, et al, *Performance of the 8-in. R5912 photomultiplier tube with super bialkali photocathode*, Journal of Instrumentation **10** (2015) T08001
- 40. X. Bertou, P. Allison, C. Bonifazi, P. Bauleo, et al. *Calibration of the surface array of the Pierre Auger Observatory*, Nuclear Instruments and Methods in Physics Research Section A: Accelerators, Spectrometers, Detectors and Associated Equipment **568** (2006) 839–846
- 41. A. Galindo, for The LAGO Collaboration, *Calibration and sensitivity of large water-Cherenkov Detectors at the Sierra Negra site of LAGO*, The 34th International Cosmic Ray Conference, volume PoS (ICRC2015) (2016) 673
- 42. The Pierre Auger Collaboration, *Studies on the response of a water-Cherenkov detector of the Pierre Auger Observatory to atmospheric muons using an RPC hodoscope*, arXiv:2007.04139 (2020)
- 43. J.J. Masías-Meza, for the Pierre Auger Collaboration, *Long-term scaler and histogram analysis*, The 34th International Cosmic Ray Conference, volume PoS (ICRC2015) (2016) 074
- 44. A.J. Rubio-Montero, R. Pagán-Muñoz, R. Mayo-García, A. Pardo-Díaz, I. Sidelnik, H. Asorey and for the LAGO Collaboration, *The EOSC-Synergy cloud services implementation for the Latin American Giant Observatory (LAGO)*, The 37th International Cosmic Ray Conference, volume PoS (ICRC2021) (2021) 261